J. Membrane Biol. 150, 89–103 (1996)

The Journal of
Membrane
Biology

Dye Transfer Between Cells of the Lens

J.L. Rae[1], C. Bartling[1], J. Rae[1], R.T. Mathias[2]

[1]Departments of Physiology and Biophysics and Ophthalmology, Mayo Foundation, Rochester, MN 55905
[2]Department of Physiology and Biophysics, SUNY, Stony Brook, NY 11794-8661

Received: 14 September 1995/Revised: 13 November 1995

Abstract. Dye transfer between lens fiber cells and between lens epithelial cells and underlying fiber cells was studied using a wide dynamic range-cooled CCD camera, H_2O immersion objectives and image analysis techniques. Each lens was decapsulated by a new technique which leaves the epithelial cells adherent to the lens fiber mass. Lucifer Yellow CH was injected into either single epithelial cells or single fiber cells using the standard whole cell configuration of the patch voltage clamp technique. The results demonstrate extensive dye communication between fiber cells at the lens posterior surface, anterior surface, and equatorial surface. Dye transfer between deep fiber cells was also observed. Dye transfer between ≈10% of epithelial cells and their underlying fiber cells was apparent when care was taken to yield wide dynamic range images. This was required because the relatively high concentration of dye in the epithelial cell masks the presence of much lower dye concentrations in the underlying fiber cell. A mathematical model which includes dye concentration, time, and spatial spread suggests that those epithelial cells that are coupled to an underlying fiber cell are about as well dye coupled as the epithelial cells themselves. The relatively low dye concentration in a fiber cell is due to its larger volume and diffusion of the dye along the axis of the fiber away from the fiber/epithelial junction.

Key words: Lens — Epithelium — Fibers — Dye transfer — Gap junctions

Introduction

Over more than 20 years, evidence has been accumulating that the lens fiber cells and even lens epithelial cells exist as a functional 3-dimensional syncytium (Duncan, 1969; Mathias, Rae & Eisenberg, 1981). In most early studies aimed at demonstrating cell-to-cell dye transfer between fiber cells or between fiber and epithelial cells, the dye transfer could be observed. In embryonic chick lenses, pathways for dye movement between fiber cells and between epithelial and fiber cells was demonstrated (Schuetze & Goodenough, 1982; Miller & Goodenough, 1986). Cell-to-cell dye movement between fiber cells of adult *Rana pipiens* lenses was also reported (Rae, 1974; Rae & Stacey, 1976) and, moreover, epithelial and fiber cells were reported to be electrically coupled in adult frog lenses (Rae & Kuszak, 1983). Several morphological studies reported the existence of gap junctions between lens epithelial and fiber cells (Goodenough et al., 1980; Miller & Goodenough, 1986; Lo & Reese, 1993).

Recently, applications of more modern imaging technology have arrived at somewhat different conclusions. While freeze fracture transmission electron microscopy easily demonstrates structures that look like gap junctions between lens fibers cells, few if any gap junctions between lens epithelial and fiber cells could be observed in a recent study (Brown et al., 1990). These results prompted several investigators (Bassnett et al., 1994) to question the existence of metabolic communication between lens epithelium and fibers. Confocal microscopy applied to intact lenses following the microelectrode injection of Lucifer Yellow CH into single fiber cells of frog lenses failed to demonstrate fiber to fiber dye movement except in a small region near the lens equator (Prescott et al., 1994). These authors also suggest that metabolic communication between fiber cells might not exist in general. Several investigators have reported that BCECF AM or SNARF-1 loaded into epithelial cells of whole lenses does not obviously pass into fiber cells and can take more than an hour to leak from

Correspondence to: J.L. Rae

the cells (Wolosin et al., 1988; Wolosin, Alvarez & Candia, 1990; Bassnett, 1990; Bassnett et al., 1994). This time period, they propose, is longer than would be expected if the dye were able to transverse gap junctions and enter the fiber cell. Bassnett et al. (1994) were able to dye fill fiber cells in embryonic chick lenses and to observe dye spread into the overlying epithelial cells. When they filled epithelial cells, however, they could not see dye move into the fiber cells below.

How are these major differences in findings to be rationalized? It is possible that the epithelial-fiber electrical coupling demonstrated by Rae and Kuszak (1983) in frog lenses might be in error. While Rae & Kuszak used a marker dye to ensure that their voltage-measuring electrode was inside a single lens epithelial cell, it may have resided somehow in a surface fiber cell. The Procion scarlet dye used to mark the position of their voltage electrode did not fluoresce appreciably and could not effectively demonstrate cell-to-cell dye transfer. Their evidence for epithelial-cell-to-fiber-cell coupling was, therefore, entirely electrical. The experiments of Schuetze and Goodenough (1982) and Miller and Goodenough (1986) did demonstrate both fiber-to-fiber and epithelial-to-fiber dye transfer but only in embryonic chick lenses. Perhaps these results do not hold for more mature lenses. The fiber-fiber dye transfer demonstrated by Rae (1974) and Rae and Stacey (1976) was done in mature frog lenses using fixed and embedded lenses and so movement of dye from cell to cell during the tissue preparation could not be ruled out though care was taken to avoid this artifact.

On the other hand, there is no paucity of artifacts or sensitivity issues which might result in failure to demonstrate cell-to-cell diffusion pathways. An intracellular microelectrode rarely has a seal around it that exceeds 100 megohms and the seal resistance can be very much lower than this. Lack of a tight seal can allow extracellular substances like Ca^{+2} to enter the cytoplasm which might result in uncoupling from adjacent cells. Moreover, in a 3-dimensional syncytium, the intensity of the dye fluorescence is expected to fall very rapidly with distance from the injection site by comparison to the expectation from either one-dimensional or two-dimensional syncytia. Thus, it would be possible for dye spread to occur but for the detection procedures to lack sufficient sensitivity to quantify or even detect the spread.

The existence of metabolic communication between lens fiber cells and between lens epithelium and fibers are important issues. We therefore chose to reinvestigate them using more modern electrophysiological approaches and more modern imaging approaches than we and most other investigators have used in the past. With these approaches, we routinely find dye transfer between fiber cells and between epithelium and fibers in several different kinds of lenses.

Materials and Methods

Preparation of the Rat Lens

Most experiments were done on lenses obtained from albino Sprague-Dawley rats (both sexes). We used rats weighing approximately 200 g because their lenses were large and relatively easy to work with. The rats were euthanized by an intraperitoneal injection of 25% urethane solution. After death, the globes were enucleated and placed in NaCl Ringer's solution at room temperature. The posterior globe was removed by cutting posterior to the zonules with fine iris scissors. The cornea and iris were then cut around their periphery and discarded. This dissection left the lens and capsule intact, attached via its zonules to a ring of uveal-scleral tissue.

Embedding the Rat Lens in Agarose

A small #184 Sylgard (Dow Corning, Midland, MI) mat (6 mm square × 2 mm thick) was used to position the lens for embedding in agarose. A #1 cork borer was used to trephine a hole in the center of the mat. The mat was submerged in NaCl Ringer's solution and the rat lens positioned over the hole using a lens loop. For most *fiber-fiber cell experiments*, the posterior of the lens fit down into the hole in the Sylgard mat; for *epithelial-fiber cell experiments*, the opposite orientation was used. A 2% weight/volume agarose solution was made, using equal amounts of SeaKem GTG and SeaPlaque agarose (FMC BioProducts, Rockland, ME) dissolved in NaCl Ringer's solution. Microwave heat was applied to dissolve the agarose. The agarose was continuously stirred and measured with a thermometer until it cooled to approximately 37°C. At this point, the Sylgard mat with the lens was carefully moved from the Petri dish containing Ringer's solution to a silicone flat embedding mold (Ted Pella, Redding, CA). Agarose solution was poured over the positioned lens, filling the embedding trough. Enough agarose was used to completely cover the lens and overflow the trough. As the agarose began to gel, a Petri dish cover was placed, without pressure, over the trough to flatten the agarose surface. Once the agarose had adequately gelled, the Petri dish cover was removed and the excess agarose was trimmed with a razor blade, squaring the sides of the agarose mold to match the sides of the embedding trough. The entire agarose mold, containing the rat lens, was carefully removed from embedding mold, and placed in a Petri dish containing NaCl Ringer's solution. Using a #5 jeweler's forceps, the Sylgard mat was carefully removed from the agarose mold, yielding an exposed portion of the rat lens.

Decapsulation of the Rat Lens

Decapsulation of the lens was necessary for patch clamping the fiber and epithelial cells of the rat lens (Dewey, Bartling & Rae, 1995). A Ca^{+2}-Mg^{+2}-free solution containing 10 mM bumetanide (Sigma Chemical, St. Louis, MO) was used to incubate the exposed portion of the lens prior to decapsulation. The agarose block was submerged in the decapsulation solution and incubated for 15–30 min at room temperature. After incubation, the agarose block was removed from the decapsulation solution and the capsule was gently teased from the exposed lens area using two pairs of #5 jeweler's forceps.

Patch Electrodes

Corning borosilicate #7052 glass was pulled on a constant temperature coil vertical puller. The electrode tips were firepolished to final resis-

tances of approximately 8 MΩ when filled with our pipette solutions. For Lucifer Yellow CH experiments, the electrode tip was filled with a lithium chloride solution and was then backfilled with a lithium chloride-Lucifer Yellow CH solution.

Patch Clamping and Dye Iontophoresis of Rat Lens Cells

The agarose block was mounted in an acrylic chamber where the block was held in place by compression. The acrylic chamber was mounted on a modified stage of a Leitz Laborlux (Rockleigh, NJ) upright epifluorescence microscope with a Leitz 25× long working-distance Hoffman modulation contrast objective. A NaCl Ringer's solution was used to bathe the exposed lens tissue during the experiments. A linear translator was used to move the electrode against an exposed cell membrane and the current was monitored while applying a 5 mV test pulse. Gentle suction was used to allow gigohm seals to form to a cell's membrane. The seal resistance was measured and gentle suction was again used to rupture the membrane patch inside the opening of the electrode tip. Rupture of the membrane patch, to achieve a *whole-cell patch clamp* configuration, allowed maximum access to the cell's interior for dye injection while minimizing the amount of dye and ion leakage at the membrane-seal interface.

Iontophoretic currents of 1 to 15 nA were applied using a PCLAMP (Axon Instruments, Foster City, CA) voltage protocol for times between 10 to 40 mins.

Solutions

The sodium chloride Ringer's solution contained (in mM): 149.2 NaCl, 4.74 KCl; 2.54 $CaCl_2$, 5 HEPES, and 5 glucose. The pH was buffered to 7.35 and the osmolarity was measured at 290 mOsm/kg. The calcium-magnesium free bumetanide solution contained (in mM): 150 $KMeSO_3$, 2 EDTA, 5 HEPES, 0.01 bumetanide, and 5 glucose. The bumetanide was added from a 10 mM stock solution in absolute ethanol. The pipette solution used with all Lucifer Yellow experiments contained (in mM): 150 LiCl, 2 EGTA, and 5 HEPES. The pH was titrated to 7.00 after adding the dye and the osmolarity was measured at 275 mOsm/kg. The Lucifer Yellow CH dye was dissolved in the lithium chloride solution to a final concentration of 5 mM.

Image Capture and Analysis

Images were captured using a MCD1000 peltier-cooled charge-coupled device (CCD) imaging system (SpectraSource Instruments, Westlake Village, CA). The system consisted of a 1024 × 1024 CCD chip array, a 16-bit digitizer, a TEC Control Unit which powered both the external cooling fans and the peltier-cooling of the CCD chip itself, and the HPC-1 software running under Microsoft Windows. Images were captured in a 16-bit 512 × 512 pixel image format, and each image was bias and flat field image-corrected (*see* below). Most images were taken with a 40×, 0.75 NA water immersion objective (Carl Zeiss, West Germany). The images not being used for quantitation were corrected for out-of-plane fluorescence by using a no-neighbors deblurring scheme described by Monck et al. (1992). Final image analysis and contrast enhancement were performed on a Sun Microsystems SPARC workstation (SUN Microsystems, Mountain View, CA) using the ANALYZE software package (Biomedical Imaging Resource, Mayo Clinic, Rochester, MN).

CCD Nonuniformity Image Correction

The images were modified by bias field subtraction and by flat field scaling to correct for imperfections in the CCD array. The bias field subtraction corrects for nonzero charge in the CCD array immediately after clearing the array and with no light applied. The bias field image was subtracted from the raw image before flat field image correction. The flat field image correction normalizes the image data for differences in photon collection efficiency for each pixel in the array. This is accomplished by multiplying each pixel's bias field-corrected value by a scale factor. The scale factor, found by imaging a uniformly illuminated field of view, is equal to the collected pixel's value divided by the average value of all the pixels in the array.

No Neighbors Deblurring Scheme

Bias field- and flat field-corrected images obtained from the HPC-1 software were processed in a custom program after undergoing file format conversion. Monck et al. (1992) have developed a deblurring scheme which utilizes a simple inverse filter to extract optically relevant data from an input image without the need for adjacent image sections. The deblurring algorithm removes out-of-focus information from an image by convolution of the in-focus image. The resultant blurred image is then multiplied by a factor of two. The image product is then subtracted from the original in-focus image, and a Wiener inverse filter convolution was used for final image sharpening:

$$I_j = [\{O_j - 2\ c\ O_j S_1\}\{S_o/(S_o^2 + a)\}]$$

where $O_j S_1$ represents the blurred in-focus image, O_j, the original in-focus image, S_1, the blurred image contrast transfer function, S_o, the in-focus image contrast transfer function, and c and a, empirical constants (typical values of 0.48 and 5.00 were used, respectively). All capital letters represent Fourier transforms of the respective point spread functions. In the calculation of S_1, a hypothetical section spacing (Dz) was used to control the sectioning thickness parameter utilized in the deblurring algorithm. The Dz parameter was typically set at 1 mm. The numerical aperture of the objective lens (0.75), the wavelength of light emitted by the fluorophore (535 nm), pixel size (0.22 μm), and the index of refraction of the objective immersion medium (water, 1.3) were also utilized as parameters in the deblurring algorithm (Monck et al., 1992).

Other Image Processing

Resultant deconvolved images were saved and transferred to the Sun Microsystems SPARCstation1 workstation running the SunOS operating system. Images were retrieved in the ANALYZE image processing and analysis program. Many of the images were further processed by an adaptive histogram equalization operation. This process adjusts the gray scale values of an image based on the localized image area histogram. The localized area consists of an 8 × 8 pixel kernel, with the resulting histogram consisting of 64 sample values. The purpose of this equalization operation is to enhance the viewable contrast in all areas of the image, without the preservation of any mathematical relationship of gray level scale. The operation creates a histogram of gray level values for each localized area kernel. The contrast is then adjusted locally within each area kernel. The gray scale for the entire image is calculated similarly to avoid any checkerboarding. A clipping fraction limits the contribution of any pixel's given gray level value, and thus reduces the enhancement of noise in the resultant image. This operation is especially effective for expanding the dynamic range of the image in regions which have subtle but significant contrast differences.

ABBREVIATIONS

A	(cm^2) area of apical face of an epithelial cell
$C_e(t)$	(mole/cm^3) epithelial cell dye concentration
$C_f(x,t)$	(moles/cm^3) fiber cell dye concentration
$C_o(x)$	(moles/cm^3) initial (t = 0) distribution of dye in a fiber cell
C_p	(moles/cm^3) pipette dye concentration
D	(cm^2/sec) dye diffusion coefficient $\approx 1.5 \times 10^6$ cm^2/sec
h	(cm) height of epithelial cell
$j_x(x,t)$	(moles/cm^2sec) dye flux along fiber cell axis
p_e	(cm/sec) fiber/epithelial gap junctional permeability
p_f	(cm/sec) fiber/fiber gap junctional permeability
S_m/V_t	(cm^{-1}) surface to volume ratio of fiber cells
t	(sec) time since removal of patch pipette from epithelial cell
u(x)	(cm/sec) velocity of convection plus conduction
U(x)	(cm/sec) velocity of convection
V_e	(cm^3) volume of epithelial cell
x	(cm) distance along fiber cell axis from epithelial junction
λ	(cm) length constant for dye diffusion along a fiber cell
τ_e	(sec) time constant for epithelial/fiber cell dye exchange
τ_f	(sec) time constant for fiber/fiber cell dye exchange

Results

EPITHELIAL-FIBER DYE TRANSFER

As shown in the analysis section (later), epithelial-fiber dye transfer is expected to be quite difficult to demonstrate. Even for substantial degrees of coupling, dye diffuses more readily along the axis of a fiber cell than across the epithelial-fiber gap junctions. Hence, there will be a large step drop in dye concentration between the epithelial cell and the fiber cell to which it is coupled. Figure 1*A* and *B* demonstrates this phenomenon. Fig. 1*A* is a largely unenhanced photograph (deconvolution only) of dye injection into a single epithelial cell of a rat lens. The exposure is such that the epithelial cell is nearly optimally exposed. The fiber cell, however, is essentially invisible. This does not mean that the fiber cell beneath does not have dye in it. Rather, the dynamic range of the image is sufficiently limited that both the epithelial cell and the fiber cell cannot be visualized simultaneously. By using a clipped amplitude histogram equalization routine (Fig. 1*B*, *see* Materials and Methods), it is possible to display the dye in the fiber cell even though its intensity is much less than that in the epithelial cell. At this level of exposure, the intensity in the fiber is only a little above background and so the image is noisy.

Integrating CCD cameras have an antibloom capability whereby the electrons filling the most highly populated wells can be removed and so prevent blooming in the most intense areas of the image. This leaves the low order 8 bits of the camera in a linear photometric range whereas the 8 high order bits respond nonlinearly with increasing light. Figure 2*A*,-*C* shows that dye in a fiber cell coupled to its overlying epithelial cell can easily be demonstrated by turning on the antibloom feature of the camera and then exposing for a 50 to 100 fold longer period than is required to image an epithelial cell. Figure 2*A* shows a rat lens epithelial cell near the equator which has been loaded with Lucifer Yellow through a patch electrode. Here the antibloom capability was not used. In this instance, it was possible to see dye in an underlying fiber cell without enhancement. This was possible because we chose to patch one of a small cluster of cells left on the fibers following decapsulation. The neighboring cells were removed by the decapsulation procedure thus decreasing the number of adjacent epithelial cells into which the injected dye might be lost. In Fig. 2*B*, the camera's antibloom feature was used and the exposure time increased until the fiber cell dye could easily be seen. In Fig. 2*C*, the clipped amplitude histogram equalization algorithm was applied to the antibloomed image. These figures show clearly that dye injected into an epithelial cell through a patch electrode ultimately diffuses into the fiber cell below. In fact, in Fig. 2*B* and *C*, dye can be seen in several underlying fiber cells. Epithelial-fiber dye transfer was seen in 29 of 83 clusters of epithelial cells near the lens pole successfully filled with Lucifer-yellow.

When the antibloom capability of the camera is used with long exposure times, a diffuse trail of dye moving in one direction only can be seen (Fig. 3*A*). Simultaneous bright field and fluorescence imaging (Fig. 3*B*) shows that the direction of the diffuse dye trail is always along the axis of the underlying fiber cells. This unidirectional movement of the dye in fibers is expected and is explained in the cartoon below (Fig. 4). The fiber/fibers which abut any single epithelial cell leave in a single direction at all epithelial locations except right at the suture. The observed apparent unidirectional movement of dye lends credence to the notion that dye is diffusing inside the fiber cells and not in the extracellular space. In the extracellular space, dye would be expected to diffuse in all directions. A second demonstration of epithelial-fiber dye transfer is shown in Fig. 5*A* (fluorescence) and Fig. 5*B* (bright field and fluorescence) at higher magnification. Here at least 3 fluorescent fiber cells can be seen underlying the epithelial cell which was the primary injection site. The bright field photomicrography (Fig. 5*B*) clearly shows that the *apparent* fiber cells from Fig. 5*A* are in fact fiber cells.

Epithelial-fiber dye transfer was easily seen in mature rat and rabbit lenses and in 14 day chick embryo lenses. These were the only lenses we tried. The coupling could be demonstrated in rat lens with carboxyfluorescein and dichlorofluorescein (*data not shown*), in addition to Lucifer Yellow. It could not be demonstrated with BCECF although when a mixture of BCECF and Lucifer Yellow was used to fill the epithelial cell, dye transfer was evident showing that BCECF did not block dye transmission. BCECF did not even diffuse into adjacent epithelial cells, either in ''intact'' lenses or in

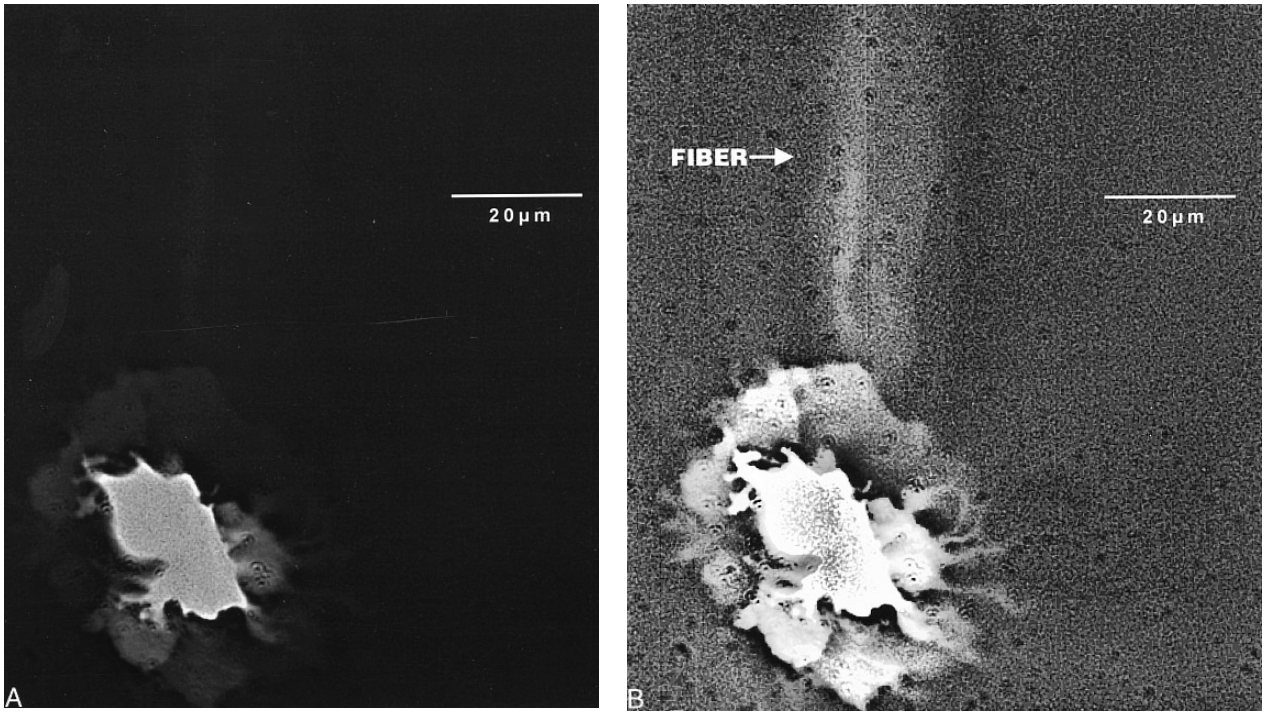

Fig. 1. CCD camera images from a rat lens wherein a single epithelial cell was dye-injected with Lucifer Yellow CH through a patch electrode used in whole cell voltage clamp mode. The image in (*A*) was deconvolved to correct for out-of-plane fluorescence. The image in (*B*) was deconvolved and subjected to clipped amplitude histogram equalization to show a noisy image of a fiber cell (*arrow*) hidden in the low order bits of the CCD camera.

dissociated cell pairs of mouse lens epithelial cells or rabbit corneal epithelial cells. Therefore, even though BCECF has been shown to diffuse between gap junctions in at least two other preparations (Cooper, Miller & Fraser, 1989; El-Sabban & Pauli, 1991), we were unable to demonstrate its movement between lens epithelial cells, between fiber cells or between epithelial and fiber cells.

The dye transfer with Lucifer Yellow was also not very dependent on the pH of pipette filling solution. Dye movement between epithelial cells and fiber cells occurred at least in a qualitatively similar way for pipette filling solution pHs between 4 and 7. Given that pH buffering can occur by H^+ movement through the gap junctions, the actual pHs which resulted in the coupled cells are not known.

These dissection, dye injection and imaging techniques also allow clear demonstration of fiber-to-fiber coupling. In Fig. 6*A* (a deconvolved image) and in Fig. 6*B* (the same image subjected to amplitude histogram equalization), extensive lateral spread of dye into posterior lens fibers adjacent to the central injection can be visualized. Results similar to these (*data not shown*) were found when dye was injected into fiber cells at both the anterior and equatorial surfaces.

We also made some attempts to inject dye into deep fiber cells using this methodology. To do that, it was necessary to mechanically peel surface fiber cells away from the rest of the lens and then patch clamp fiber cell surfaces exposed deep in the lens by the surface-fiber removal. Figure 7 shows that even under these potentially mechanically traumatic conditions, fiber-to-fiber dye movement is still readily observed. Its extent does not seem to be nearly as pronounced as between fiber cells near the lens surface but the two locations should probably not be compared directly given the anticipated mechanical trauma involved in isolation of deep fiber cell surfaces.

Analysis of the Data

Figure 8 compares the initial fluorescence intensity in three typical experiments where the introduction of dye was into an epithelial cell either at the pole, midway between pole and equator, or at the equator. The fluorescence intensity as a function of position along the fiber cell axis is not a simple exponential. One reason for the complex distribution may be the shape of the fiber cells. We measure fluorescence intensity, which is proportional to the amount of dye at any x location rather than the concentration of dye. Thus, where the fiber cells are thicker we will collect more light even if the concentration is not higher. At the equator, the fiber

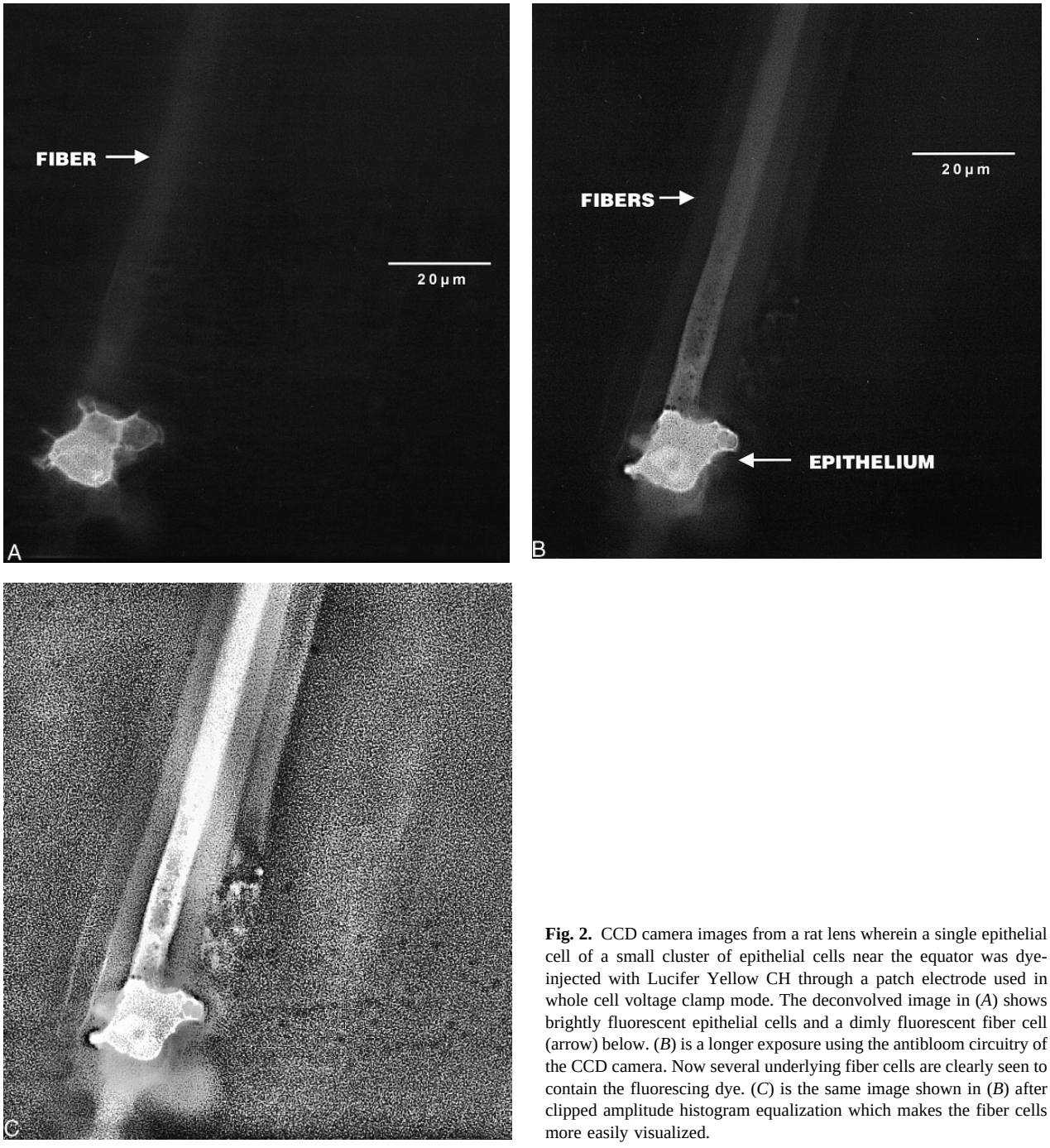

Fig. 2. CCD camera images from a rat lens wherein a single epithelial cell of a small cluster of epithelial cells near the equator was dye-injected with Lucifer Yellow CH through a patch electrode used in whole cell voltage clamp mode. The deconvolved image in (*A*) shows brightly fluorescent epithelial cells and a dimly fluorescent fiber cell (arrow) below. (*B*) is a longer exposure using the antibloom circuitry of the CCD camera. Now several underlying fiber cells are clearly seen to contain the fluorescing dye. (*C*) is the same image shown in (*B*) after clipped amplitude histogram equalization which makes the fiber cells more easily visualized.

cells are more banana-shaped than at the poles, so the increase in intensity as one moves away from the fiber/epithelial junction could simply be an artifact due to the shape. Secondly, forces other than diffusion may contribute to dye spread. As first reported by Robinson and Patterson (1983) there are circulating currents between the pole and equator and these currents will generate conduction and convection of dye. Based on an analysis of these currents (Baldo & Mathias, 1992), the voltage and hydrostatic pressure in peripheral fiber cells at the equator will be higher than in peripheral cells at the poles, hence the negatively charged dye will be conducted toward the equator but convected toward the poles. The longitudinal flux of dye along the axis of a fiber cell is given by

$$j_x(x,t) = -D\,\frac{\partial C_f(x,t)}{\partial x} + C_f(x,t)\,u(x)\,\frac{\text{moles}}{cm^2 sec} \qquad (1)$$

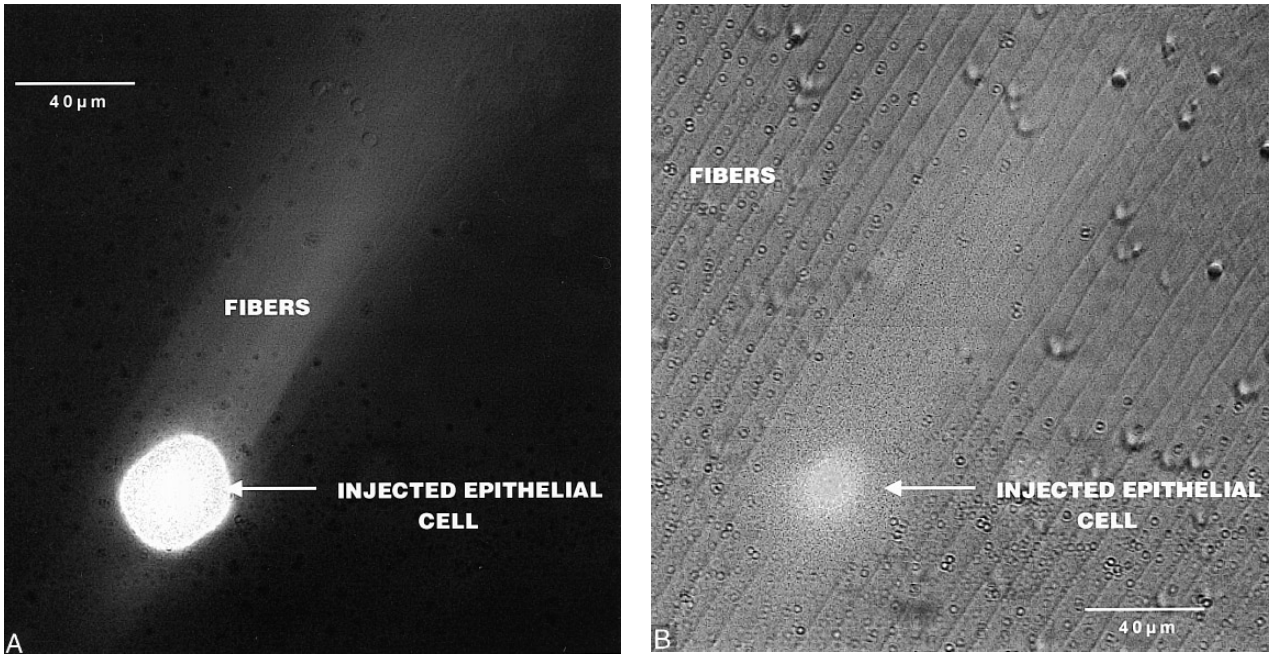

Fig. 3. (*A*) A deconvolved CCD camera image from a rabbit lens wherein a single epithelial cell was filled with Lucifer Yellow CH through a patch electrode used in whole cell voltage clamp mode. Antibloom circuitry of the camera was used with a sufficiently long exposure time to render the underlying fiber cell fluorescence visible. The epithelial cells are overexposed and appear saturated. (*B*) A bright field image of the same microscopic field shown in (*A*) to verify that the fiber fluorescence band in (*A*) follows the same orientation as that of the fiber cells.

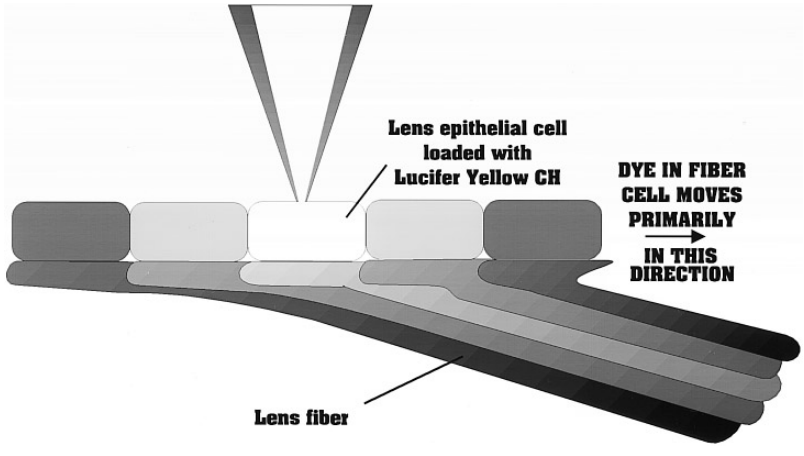

Fig. 4. A cartoon of the fiber cell orientation with respect to the epithelial cell location in a decapsulated lens. Dye in a fiber cell would move along the fiber axis but would seem to move primarily from left to right. The movement would appear largely unidirectional.

where $C_f(x,t)$(mmoles/cm^2) is the dye concentration at location x (cm) and time t (sec) in a fiber cell, D (cm^2/sec) is the dye diffusion coefficient and the velocity u(x) (cm/sec) represents either conduction or convection. Viz

$$u = -D\frac{Fz}{RT}\frac{d\psi(x)}{dx} + U(x) \text{ cm/sec} \tag{2}$$

The voltage within the fiber cell is $\psi(x)$ and $U(x)$ (cm/sec) is the fluid flow velocity. Other symbols and coordinates are defined in Fig. 9. Positive values of x are defined along the axis of the fiber cell as distance from the epithelial/fiber junction. The longitudinal flux at the fiber/epithelial junction must equal the transjunctional flux, which is given by $p_e(C_e(t) - C_f(0,t))$, where p_e (cm/sec) is the fiber-epithelial junctional permeability. Since $C_e(t) >> C_f(0,t)$, we can approximate

$$p_e C_e(t) \simeq -D\frac{\partial C_f(0,t)}{\partial x} + u(0)C_f(0,t) \tag{3}$$

Eq. 3 can be rewritten as

$$D\frac{\partial C_f(0,t)}{\partial x} = u(0)C_f(0,t) - p_{eC_e}(t) \tag{4}$$

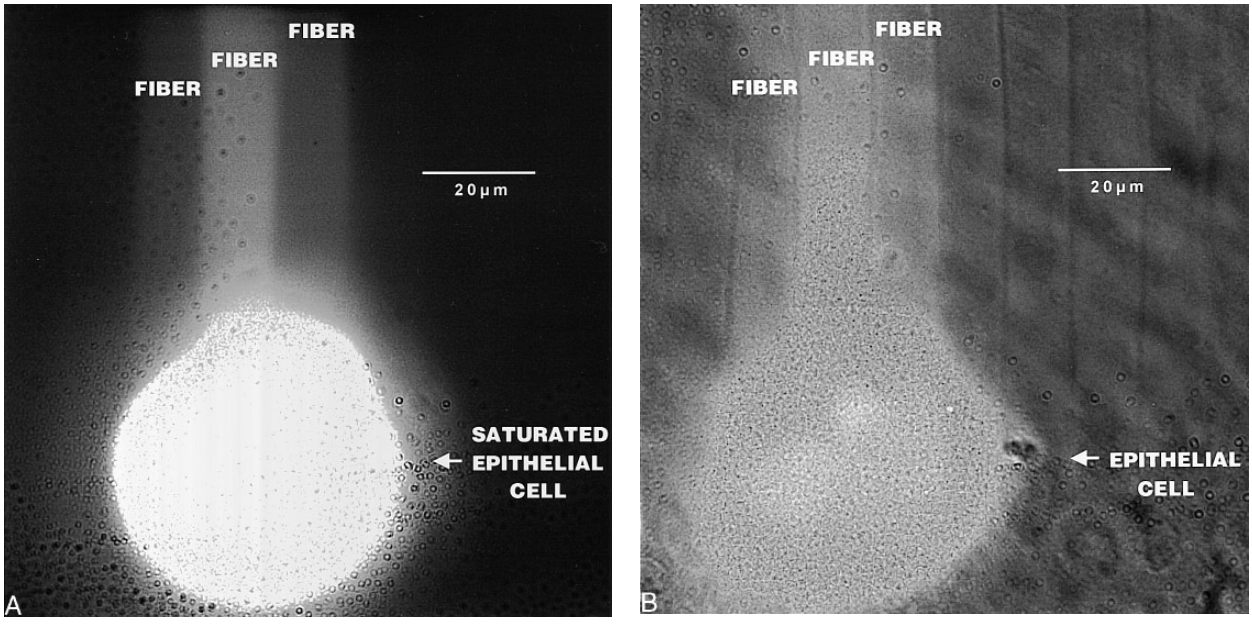

Fig. 5. (*A*) A higher magnification CCD camera image of a rat lens in which a single lens epithelial cell was injected with Lucifer Yellow CH through a patch electrode used in whole cell voltage clamp mode. Antibloom circuitry of the camera and a long exposure time were used to allow visualization of fluorescing dye in fiber cells below. (*B*) A brightfield micrograph of the same microscopic field shown in (*A*) to demonstrate that the apparent fiber cells of (*A*) are really fiber cells.

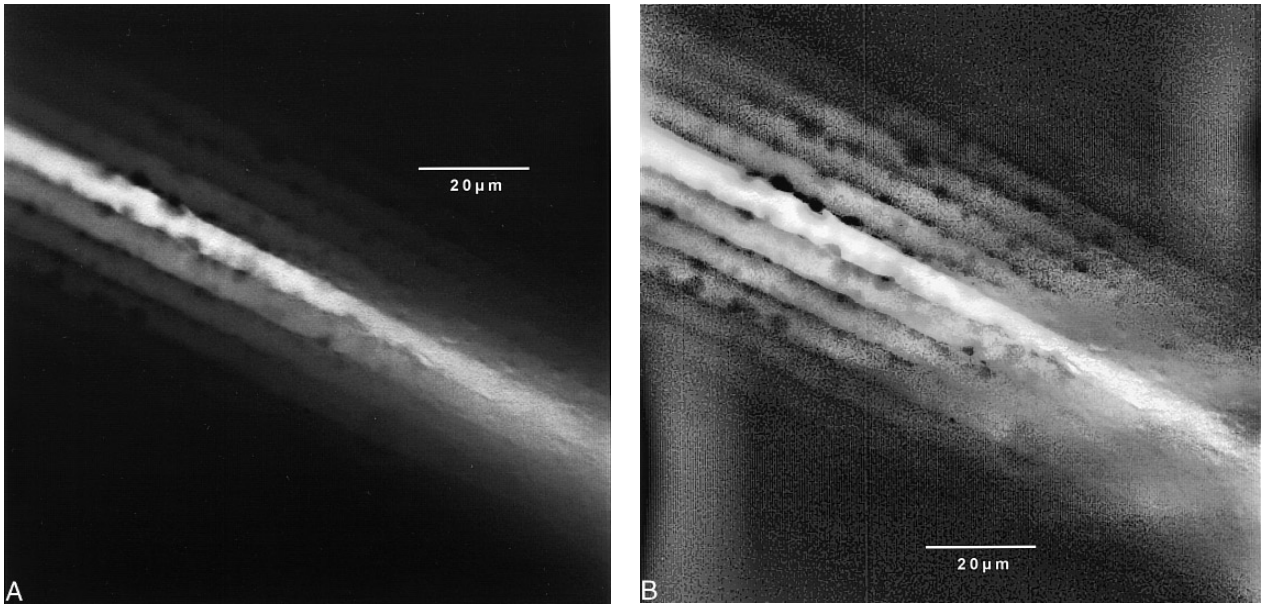

Fig. 6. (*A*) A deconvolved CCD camera image from a rat lens in which Lucifer Yellow CH was injected into a surface fiber cell at the posterior surface between the equator and the posterior pole. A path electrode in whole cell voltage clamp mode was utilized. Diffusion of the fluorescing dye into adjacent fiber cells is clearly visible. (*B*) The same image from (*A*) following clipped amplitude histogram equalization. This enhancement shows that dye can be seen in even more cells than in (*A*).

At the poles, the data show $\partial C_f(0,t)/\partial x$ is negative hence u is either small or negative. Since conduction carries the dye away from the poles whereas convection carries dye to the poles, the convection velocity, $U(x)$, is negative and may dominate. At the equator, $\partial C_f(0,t)/\partial x$ is positive, suggesting $u(0)$ is positive and large. In this situation, x is increasing as we move away from the equator so convection is positive whereas conduction is

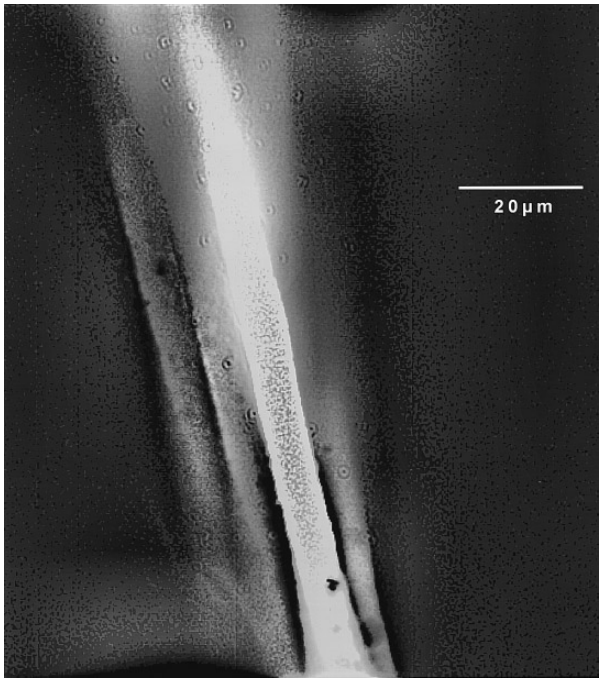

Fig. 7. A deconvolved and clipped amplitude histogram equalized CCD camera image from a microdissected rat lens. A single deep fiber cell was injected with Lucifer Yellow CH through a patch electrode used in whole cell voltage clamp mode. Dye spread into adjacent fiber cells is apparent.

negative so again $U(x)$ may dominate. The data are therefore consistent with a significant flux of dye being carried by convection, which contributes to the complex longitudinal distribution of fluorescence intensity.

In the analysis that follows, we will focus on data collected near the anterior pole. Data from the equator or midway from pole to equator have qualitatively the same behavior but are more erratic, so curve fits are neither as good nor as consistent. We have two viable explanations for the data so we will undertake an analysis that allows for either. $u(x)$ is included in the equations as an unspecified function so for a pure diffusion model, $u(x)$ can be set to zero. An approximate solution can be found even without specifying $u(x)$. This is possible only because of a specific feature of the data: as can be seen in Fig. 10*A*, the x-distribution of fluorescence intensity does not change shape with time, rather it diminishes at the same rate at each x. Moreover, the time course at each x is a simple exponential as shown in Fig. 10*B*, where the fluorescence intensity at 20 μm intervals is graphed as a function of time and the data fit with a simple exponential. For reasons described below, that $t = 0$ point, representing the time at which the patch electrode was withdrawn from the cell, was excluded from the curve-fit. The best fit time constants at each x are listed on the graph and one can see they are consistently around 25 mins. We will show this behavior implies dye is lost laterally to neighboring fiber cells and the rate limiting step is diffusion of dye from the epithelial cell into the fiber cell. This loss of dye concentration with time cannot be explained by bleaching. Single epithelial cells or pairs of epithelial cells dye injected with Lucifer Yellow and exposed to light of the same intensity for the same time as ''intact'' preparations lose less than 2–5% of their intensity by bleaching.

Define the initial distribution of dye in the fiber cell as $C_o(x)$. We observe $C_o(x)$ is independent of the time of filling the cells (in the range of 7 min to 15 min) so a steady-state is achieved by 7 min. However, $C_o(x)$ varies considerably in shape as one looks from pole to equator. If the pipette contains a concentration of dye C_p, the initial concentration in the epithelial cells will be very close to C_p. Thus, we assume

$$C_e(0) = C_p$$
$$C_f(x,0) = C_o(x) \tag{5}$$

$$\frac{d\, V_e C_e(t)}{dt} = -A p_e C_e(t) \tag{6}$$

The volume of an epithelial cell, V_e(cm^3), is given by its apical area A (cm^2) times its height h (cm). Once the pipette is removed, the amount of dye in the epithelial cell declines as the dye diffuses through the apical junctions into the fiber cells. Thus, since V_e is constant, we divide through and obtain the time constant

$$\frac{dC_e(t)}{dt} = -\frac{1}{T_e} C_e(t),\ T_e = h/p_e \tag{7}$$

With the initial condition in Eq. 5, the solution is

$$C_e(t) = C_p e^{-t/T_e} \tag{8}$$

In the fiber cell, dye is continually gained from the epithelial cell but continually lost through lateral gap junctions to neighboring fibers. If the lateral junctional permeability is p_f(cm/sec), and the surface to volume ratio of the fiber cell is S_m/V_T, then the time constant is

$$T_f = 1/\frac{S_m}{V_T} p_f \tag{9}$$

For simplicity, we ignore the effect of dye in neighboring fiber cells and write

$$\frac{\partial C_f(x,t)}{\partial t} = D\frac{\partial^2 C_f(x,t)}{\partial x^2} - \frac{\partial (u(x) C_f(x,t))}{\partial x} - \frac{1}{T_f} C_f(x,t) \tag{10}$$

The initial condition is given by Eq. 5, the boundary condition by Eq. 3, and we assume $C_f(x,t) \to 0$ as $x \to \infty$.

If we normalize time with respect to the epithelial-

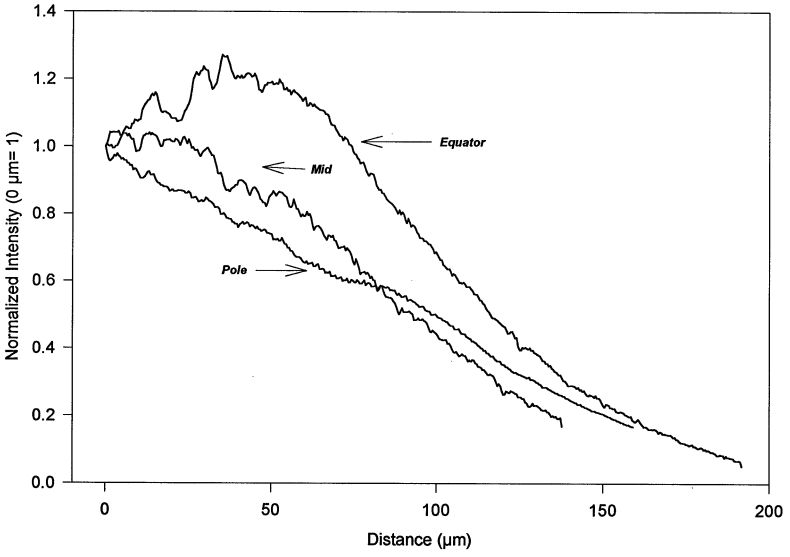

Fig. 8. A comparison of $C_f(x)$ at pole, mid, and equator illustrating the nonexponential distribution and the systematic variation in distribution.

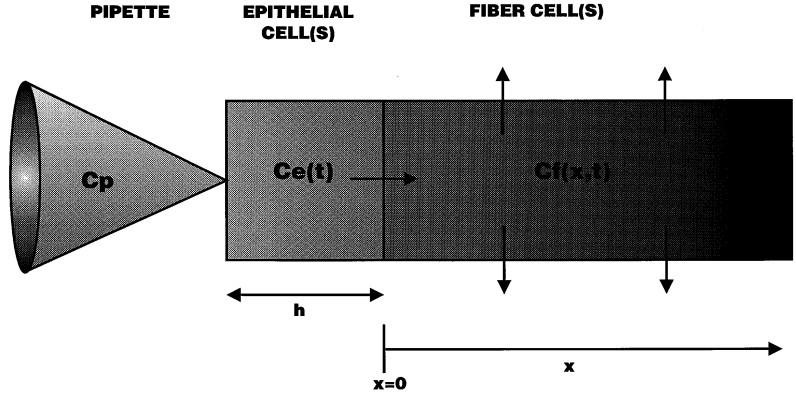

Fig. 9. A schematic drawing of the geometry, the concentration in each compartment, and the paths of dye flux. We assume dye concentration in the epithelial cells is spatially uniform, initially fills from the pipette to a value C_p, then declines with time as dye diffuses into the fiber cells. Dye in the fiber cells is gained from the epithelial cells but lost laterally to neighboring fiber cells giving a distribution of concentration over *x*.

fiber junctional time constant τ_e, then the time derivative in Eq. 10 is multiplied by the ratio τ_f/τ_e. If this ratio is small, viz

$$\frac{T_t}{T_e} \to 0 \tag{11}$$

then Eq. 10 simplifies to

$$0 \approx T_f D \frac{\partial^2 C_f}{\partial x^2} - T_f \frac{\partial (u\, C_f)}{\partial x} - C_f \tag{12}$$

The solution of Eq. 12, with initial condition given in Eq. 5 and boundary condition in Eq. 3 & 8, is

$$C_f(x,t) = C_o(x) e^{-t/T_e}$$
$$C_e(t) = C_p\, e^{-t/T_e} \tag{13}$$

In other words, when the slowest, rate-limiting step is the time constant τ_e for diffusion of the dye into the fiber cell, then dye will be lost through lateral junctions at the same rate it diffuses into the fiber and the shape of the *x*-distribution will not change with time. However, because $u(x)$ is an unspecified function, we cannot write an analytical expression for $C_o(x)$. In the special case where $u = 0$, the problem can be solved completely. Analysis of this situation shows the problem involves two time scales and the solution in Eq. 13 is only valid at long times when terms which depend exponentially on t/τ_f have died out. The long time solution is then

$$C_f(x,t) = \frac{\lambda p_e}{D} C_p e^{-x/\lambda} e^{-t/T_e} \quad u(x) = 0$$

$$\lambda = \sqrt{T_f D} \tag{14}$$

$$C_e(t) = C_p e^{-t/T_e}$$

For data analysis, it is better to utilize all of the *x* locations so we integrate Eq. 14 over *x* to obtain

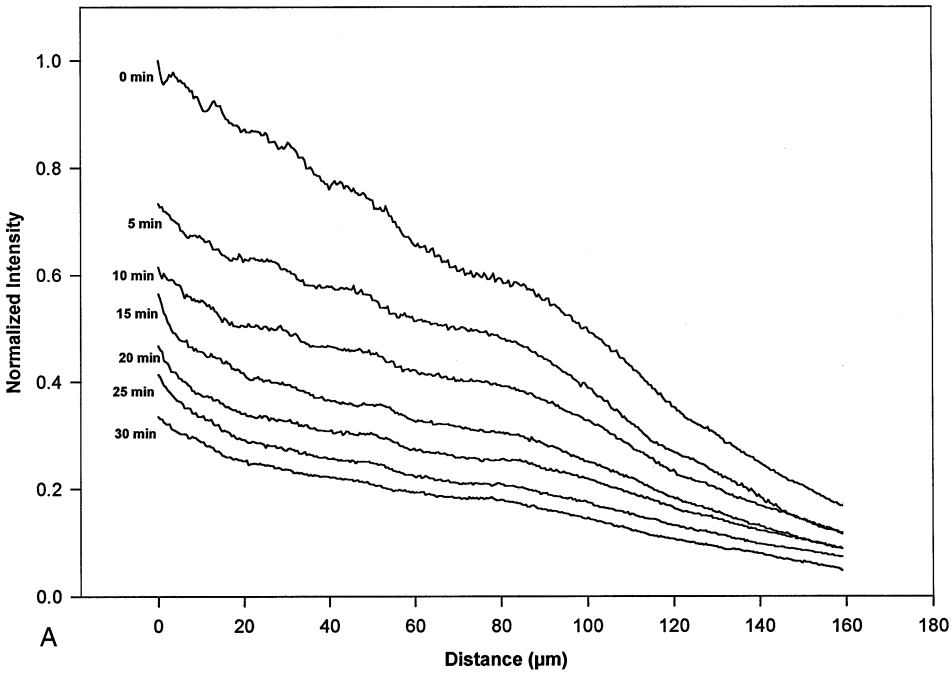

Fig. 10. Representative data from the pole showing the distribution $C_f(x,t)$ at various t (*A*) and the time course of various x (*B*). The x-distribution does not change shape with time. Best fit time constants for each x are shown. The average tau from all pole data was 25.7 ± 4.1 min.

$$\int_0^\infty C_f(x,t)dx/C_e(t) = p_e/D \tag{16}$$

$$\int_0^\infty C_f(x,t)dx = \frac{P_e}{D} C_p e^{-t/T_e} \tag{15}$$

Fig. 11 illustrates the time course of $C_e(t)$ and the time course of the integral in Eq. 15. The data are average values from 4 experiments in which the fluorescence in both the epithelial and fiber cell were recorded. An exponential was fit to the data, however, the first ($t = 0$) point was excluded from the fit because the analysis suggested our solution is valid only after terms which depend on e^{-t/ι_e} have died out. The time constant from the epithelial cells was 26 ± 1 min and from the fiber cells 24 ± 2 min. As assumed in this analysis, the time constants are essentially the same. This result is expected whether or not $u(x)$ contributes to $C_f(x,t)$ as long as τ_f/τ_e is small. We can now compare these equations with the data to estimate the parameters of interest. From all of the data on $C_e(t)$ and the integral of $C_f(x,t)$, the average value of τ_e is

$$T_e \simeq 26 \pm 3 \text{ min } (N = 14) \tag{18}$$

If we estimate a value for h, p_e can be determined from τ_e using Eq. 7.

$$h \simeq 10\ \mu m\ , \tag{}$$

$$p_e \simeq (0.6 \pm 0.07) \times 10^{-6} \text{ cm/sec} \tag{19}$$

The above results are independent of the value of $u(x)$. In the special case where $u(x)$ is small or zero, we can use Eq. 16 to determine p_e from data on the ratio

$$\int_0^\infty C_f(x,t)dx/C_e(t) = 2.9 \pm 2.3 \quad (N = 4) \tag{20}$$

The value of D is approximately

$$D = 1.5 \times 10^{-6} \text{ cm}^2\text{/sec (Brink \& Ramanan, 1985)} \tag{21}$$

which yields

$$p_e = (4.4 \pm 3.5) \times 10^{-6} \text{ cm/sec} \tag{22}$$

Though the value of p_e in equation 21 is based on $U(x)$ being negligible, it is in reasonable agreement with equation 18, which contains no assumptions on $U(x)$ and employs independent data to estimate p_e. An estimate of τ_f can be obtained from the length constants in Fig. 10*A*. Although none of the x-distributions of fluorescence intensity are simple exponentials, they all decline to about 33% of their initial value in a distance of about 100 μm. If we assume this characteristic length is representative of the length constant in Eq. 14, then for

$$\lambda \simeq 100\ \mu\text{m}, \tag{23}$$

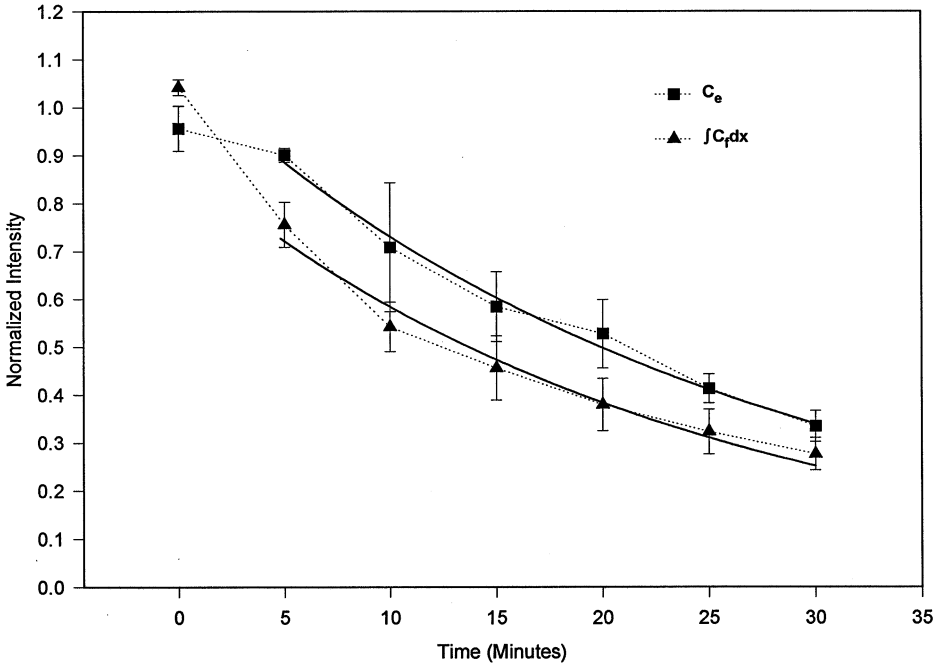

Fig. 11. A comparison of $C_e(t)$ and $C_f(x,t)dx$ (at pole) illustrating the similarity of the time constants. The data are average normalized values from four experiments in which fluorescence in both the epithelial and fiber cell were recorded. The average time constant from all $C_e(t)$ data is 26 ± 1 min and from the fiber cells is 24 ± 2 min. The average ratio $C_f\,dx/C_e$ was 2.9 ± 2 min.

the above value of D given

$$T_f \simeq 1 \text{ min} \tag{24}$$

Lastly, from Mathias, Rae and Eisenberg (1979) we estimate S_m/V_T and then calculate p_f from τ_f using Eq. 9.

$$S_m/V_T \simeq 6000 \text{ cm}^{-1}$$
$$p_f \simeq 2.8 \times 10^{-6} \text{ cm/sec} \tag{25}$$

It is of interest to estimate how the above permeabilities compare to values of gap junctional conductance reported by Cooper, Rae & Gates (1989) or Duncan et al. (1988) for frog lens epithelial cells. The comparison, however, must take into account the very large difference in size of K^+ or Cl^- (molecular weights of 39 and 35 respectively) *vs.* that of Lucifer Yellow (molecular weight 521.6). In the simplest case, one can assume permeability is proportional to the diffusion constant, which reflects the size and mobility of the solute. Based on this assumption, the fiber cell junctional permeability for KCl, $_{\text{PKCl}}$, should be at least 10-fold greater than p_f in Eq. 24, hence we estimate

$$p_{\text{KCl}} = 28 \times 10^{-6} \text{cm/sec} \tag{26}$$

Conductance depends on the concentration of permeant ions as well as their permeability. The total intracellular concentration of KCl is approximately

$$C_K + C_{\text{Cl}} \simeq 160 \text{ mM} \tag{27}$$

Thus, the expected junctional conductance is

$$G_j \simeq \frac{F^2(C_K + C_{\text{Cl}})}{RT} p_{\text{KCl}} \simeq 0.02 \text{ S/cm}^2 \tag{28}$$

Cooper et al. (1989) report an average coupling conductance between pairs of frog lens epithelial cells of 65 nS. These cells are approximately hexagonal with a height of 8 μm and a width of 20 μm, thus the area of contact between cells is around 93 μm^2 and the conductance per area of contact is 0.07 S/cm^2. Duncan et al. (1988) report an effective intracellular resistivity of 2500 Ω cm for sheets of frog lens epithelial cells. Since current must cross a junction every 20 μm, their data suggest a conductance of 0.2 S/cm^2. Given the different methods and number of assumptions involved in making this comparison, the values agree rather well. We conclude the fraction of epithelial cells that are coupled to underlying fibers are well coupled. The relatively low concentration of dye in the fiber cells is not because the epithelial/fiber permeability is small, rather it is a consequence of the relatively large volume of the fiber cell and the lateral loss of dye to the mass of surrounding fiber cells.

Discussion

For these studies we have used a different biological preparation, different electrophysiological approaches,

and different imaging methodology than have previously been used to investigate dye transfer between lens cells. The biological preparation is a new one in which we use a calcium-and magnesium-free incubation solution containing EDTA and bumetanide to decapsulate the lens while leaving the epithelial cells attached to the fiber cells. By adjusting the incubation time in the decapsulation fluid, it is possible to decapsulate the lens with *all* epithelial cells adhering to the fiber cells, *no* epithelial cells adhering to the fiber cells, or some combination in between. When only a fraction of the epithelial cells is left adherent to the fiber mass, small clumps of epithelial cells can be dye injected. Because the number of lateral cells into which dye might diffuse is limited, it is possible to get higher concentrations of dye within the cells in the clump than would have been possible with a fully intact epithelium. The dye is injected using patch voltage clamp techniques. Lucifer Yellow filled electrodes are sealed to the cells in the whole cell recording mode where dye can either diffuse and/or be electrophoresed into the cells using patch clamp electronics. This approach has the advantage that virtually no leak exists around the patch electrode and consequently the flux of calcium through the seal and the resulting increase in intracellular calcium does not occur. Because of the large cross-sectional area of the tip, it is possible to inject more dye per unit time than is possible with the much smaller intracellular microelectrodes used for intracellular dye injection. One must be careful with this approach, however, because it is easily possible to put so much dye in the cells that they take up water from the bathing solution and explode. This technique also has the potential disadvantage that it can wash out regulatory substances that exist inside of the cell since the large volume of the pipette in comparison to the volume of the cell ensures that the cell largely takes on the composition of the pipette filling solution. We also employ wide dynamic range imaging by using a cooled CCD camera with a 16-bit gray scale digitization. Under proper conditions, this allows both bright objects and dim objects to be imaged simultaneously.

These studies show that unlike recently published studies of dye transfer between fiber cells (Prescott et al., 1994), fiber cells at least at the lens surface are exceptionally well coupled. In a few attempts aimed at demonstrating dye transfer between fiber cells at least 1 mm or so deep into the lens, it was easily possible to demonstrate some lateral movement of the dye from cell to cell. These patch clamp methods, however, are not well suited to measuring dye transfer deep in the lens since surface layers of the lens must be mechanically removed and may result in damage of the fibers below. Even given this potential for damage, lateral dye cell coupling was routinely seen. Dye transfer between fiber cells at the surface, whether at the posterior surface, equatorial surface, or anterior surface was extensive. These results are in keeping with previous intracellular microelectrode studies from frog lenses (Rae, 1974; Rae & Stacey, 1976) and chick embryo lenses (Schuetze & Goodenough, 1982; Miller & Goodenough, 1986) but are not in keeping with recent results from confocal microscopy in the frog lens (Prescott et al., 1994).

Our studies also show that the epithelium is coupled to the fiber cells below by pathways that allow dye movement. In fact, a crude model aimed at quantifying the extent of dye transfer suggests that the epithelium and fibers are exceptionally well coupled, about as well coupled as the epithelial cells are among themselves. This result was true in lenses of all species in which it was studied that included rat lenses, rabbit lenses, and embryonic chick lenses. Fiber-epithelial dye transfer was seen in 29 of 83 successful experiments in which an epithelial cell was filled with Lucifer Yellow. Therefore, the fraction of total epithelial cells coupled to fiber cells should not exceed 0.35. This fraction is likely an overestimate because with every epithelial cell injection, there are 3–4 adjacent epithelial cells that take up enough dye through epithelial-epithelial gap junctions that they could serve as dye sources for demonstrating dye transfer into the fiber cell immediately below them. Therefore, in the 54 attempts in which epithelial-fiber dye transfer was not observed, one would have expected to see dye transfer into about two fiber cells/attempt if the fraction of cells coupled was 0.35. This was never observed. Rather, dye transfer is seen in one of three attempts where 3–4 cells were available to demonstrate coupling/attempt. This represents a coupling fraction of .067–.08 or less than 1 epithelial cell in 10 is coupled to a neighboring fiber cell. This coupling fraction does not alter the notion that the epithelial cells and fiber cells exist in a 3-D syncytium. Since the epithelial cells are themselves well coupled, not every epithelial cell must be connected directly to its underlying fiber cell for the syncytial connections to be complete. Moreover, these results are from the polar region of the epithelium and Baldo and Mathias (1992) showed fiber cell coupling is much less at the polar region. Epithelial cell coupling could be similarly reduced but we were unable to obtain enough data from the equatorial region to produce a reasonable comparison.

The analysis of epithelial-fiber cell coupling shows it is anticipated (and found experimentally) that there is a large concentration difference between the epithelial cell and the fiber cell below. This dye concentration difference does not then provide evidence that the cells are poorly coupled. The large drop in concentration depends primarily on the fact that the underlying fiber cells are exceptionally well coupled and are of much larger volume than the epithelial cells above.

How then are we able to rationalize these results with previous morphological and electrophysiological results that suggest little or no coupling between the

epithelial cells and fiber cells and between the fiber cells themselves? First, consider the results of Bassnett et al. (1994) in which they were able to easily demonstrate dye transfer between fiber and epithelium when the dye was injected in the fiber cell but could not demonstrate it when the dye was injected in the epithelial cell of embryonic chick lenses. These results are expected. A loaded fiber cell would offer a nearly infinite source of dye to diffuse into the epithelial cells above. Injecting dye into the epithelial cell results in an extremely low dye concentration in the fiber cells below, a concentration which could have easily have been missed without the application of the wide dynamic range imaging we utilize here. In fact, using our procedures we were able to inject Lucifer Yellow into embryonic chick lens epithelial cells and see dye movement into fiber cells below (*data not shown*).

The methods which we use are incapable of identifying morphologically or biochemically the pathway that gives rise to the dye movement from epithelial cells to fiber cells. They can, however, clearly demonstrate that a pathway exists. The work of Bassnett et al. (1994) did not conclude that such pathways did not exist, only that the pathways are rare or are morphologically different from classical gap junctions. Our results, that less than 1 in 10 epithelial cells are connected to fibers, suggests that the pathways are quite rare, at least in the anterior polar region.

Another possibility for failure to demonstrate dye transfer between epithelial cells or epithelium and fiber cells might result from the well-known fact that intracellular microelectrodes even with tips smaller than 0.1 μm in diameter rarely have more than a 100 megohm seal around them. Influx of calcium ion or some other substance from the bath might simply result in uncoupling and failure to demonstrate cell to cell dye movement. Our methods, where we inject dye through a patch clamp electrode, greatly reduce this leak problem but might wash out vital control substances and induce coupling that did not exist normally. This result would certainly be contrary to that obtained, for example, from cell pair measurements of lens epithelial cells (Cooper et al., 1989) or many other types of cells in which the washout of substances inherent in the patch clamp technique results in uncoupling of the cells with time and not the production of a coupling pathway that did not previously exist.

Previous reports that lens epithelial cells loaded with BCECF do not lose their dye to the fiber cells over time (Wolosin et al., 1988, 1990; Bassnett et al., 1994) can easily be explained by our observations that BCECF diffuses poorly through lens gap junctions if at all. BCECF (MW = 520) is larger than Lucifer Yellow and more negatively charged (4–5 charges at physiological pH) and so may exceed some size/charge maximum for movement between these cells. We cannot unequivocally rule out the possibility that our procedures disrupt the pathways for BCECF movement. But, if so, they may be different pathways than for Lucifer Yellow since dye continues to move when a mixture of BCECF and Lucifer Yellow fills an epithelial cell. Of course, Lucifer Yellow might somehow reopen pathways for BCECF movement closed by BCECF. Our experiments do not allow a distinction between the two mechanisms. However, unlike the experiments of Bassnett et al. (1994), we were able to demonstrate epithelial to fiber diffusion of carboxyfluorescein and dichlorofluorescein. We did not try SNARF-1, another dye which Bassnett (1990) and Bassnett et al., (1994) concluded could not move from epithelial cells to fiber cells.

The results that we report here are very much in keeping with early dye diffusion measurements from embryonic lens epithelial and fiber cells and from electrical measurements which demonstrate electrical coupling between the epithelium and fibers in frog lenses. We believe that the best explanation for the data presented here is that about 10% of the epithelial cells and polar surface fiber cells are in dye communication and that the cells that are coupled are very well coupled. The model used for analyzing the data suggests that the epithelial cells that are coupled to the fiber cells are coupled almost as well as the epithelial cells are coupled to each other.

We are grateful to Helen Hendrickson and Jerry Dewey for technical help and to Julio Fernandez and Jonathan Monck for help with the nearest neighbor analysis and to Erika Wohlfiel for help in preparing the manuscript. The work was supported by NIH grants EY03282, EY06005 (JLR), EY06391 (RTM), and by an unrestricted award from Research to Prevent Blindness.

References

Baldo, G.J., Mathias, R.T. 1992. Spatial variations in membrane properties in the intact rat lens. *Biophys. J.* **63:**518–529

Bassnett, S. 1990. Intracellular pH regulation in the embryonic chicken lens epithelium. *J. Physiol.* **431:**445–464

Bassnett, S., Kuszak, J.R., Reinisch, L., Brown, H.G., Beebe, D.C. 1994. Intercellular communication between epithelia and fiber cells of the eye lens. *J. Cell Science* **107:**799–811

Brink, P.R., Ramanan, S.V. 1985. A model for the diffusion of fluorescent probes in the septate giant axon of the earthworm: Axoplasmic diffusion and junctional membrane permeability. *Biophys. J.* **48:**299–309

Brown, H.G., Pappas, G.D., Ireland, M.E., Kuszak, J.R. 1990. Ultrastructural, biochemical, and immunologic evidence of receptor-mediated endocytosis is in the crystalline lens. *Invest. Ophthalmol. Vis. Sci.* **111:**2579–2592

Cooper, M.S., Miller, J.P., Fraser, S.E. 1989. Electrophoretic repatterning of charged cytoplasmic molecules within tissues coupled by gap junctions by externally applied electric fields. *Develop. Biol.* **132:**179–188

Cooper, K., Rae, J.L., Gates, P. 1989. Membrane and junctional properties of dissociated frog lens epithelial cells. *J. Membrane Biol.* **111:**215–227

Dewey, J., Bartling, C., Rae, J.L. 1995. A non-enzymatic method for

lens decapsulation which leaves the epithelial cells attached to the fibers. *Curr. Eye Res.* **14:**357–362

Duncan, G. 1969. The site of the ion restricting membranes in the toad lens. *Exp. Eye Res.* **8:**406–412

Duncan, G., Stewart, S., Prescott, A.R., Warn, R.M. 1988. Membrane and junctional properties of the isolated frog lens epithelium. *J. Membrane Biol.* **102:**195

El-Sabban, M.E., Pauli, B.U. 1991. Cytoplasmic dye transfer between metastatic tumor cells and vascular endothelium. *J. Cell Biol.* **115:**1375–1382

Goodenough, D.A., Dick, J.S.B. II, Lyons, J.E. 1980. Lens metabolic cooperation. A study of mouse lens transport and permeability visualized with freeze-substitution autoradiography and electron microscopy. *J. Cell Biol.* **86:**576–589

Lo, W.K., Reese, T.S. 1993. Multiple structural types of gap junctions in mouse lens. *J. Cell Sci.* **106:**227–235

Mathias, R.T., Rae, J.L., Baldo, G.J., Shi, J. 1989. Electrical properties of structural components of the lens. A comparison of frog and rat lenses. *Invest Ophthalmol. Vis. Sci.* **30:**(Suppl), 87

Mathias, R.T., Rae, J.L., Eisenberg, R.S. 1981. The lens as a nonuniform syncytium. *Biophys. J.* **34:**61

Mathias, R.T., Riquelme G., Rae J.L. 1991. Cell to cell communication and pH in the frog lens. *J. Gen. Physiol.* **98:**1085–1103

Miller, T.M., Goodenough, D.A. 1986. Evidence for two physiologically distinct gap junctions expressed by the chick lens epithelial cell. *J. Cell Biol.* **102:**194–199

Monck, J.R., Oberhauser, A.F., Keating, T.J., Fernandez, J.M. 1992. Thin-section ratiometric Ca2+ images obtained by optical sectioning of fura-2 loaded mast cells. *J. Cell Biol.* **116:**745–759

Prescott, A., Duncan, G., Van Marle, J., Vresen, G. 1994. The correlated study of metabolic cell communication and gap junction distribution in adult frog lens. *Exp. Eye Res.* **58(6):**737–746

Rae, J.L., Kuszak, J.R. 1983. The electrical coupling of epithelium and fibers in the frog lens. *Exp. Eye Res.* **36:**317–326

Rae, J.L. 1974. The movement of procion dye in the crystalline lens. *Invest. Ophthal.* **13:**147–150

Rae, J.L., Stacey, T. 1976. Intracellular markers in the crystalline lens of the rat. Documenta Ophthalmologica Proceedings Series. *In:* Progress of Lens Biochemistry Research. O. Hockwin, editor. pp. 233–239. Dr. W. Junk b.v., The Hague

Robinson, K.R., Patterson, J.W. 1983. Localization of steady currents in the lens. *Curr. Eye Res.* **2:**843–847

Schuetze, S.M., Goodenough, D.A. 1982. Dye transfer between cells of the embryonic chick lens becomes less sensitive to CO_2 treatment with development. *J. Cell Biol.* **92:**694–705

Wolosin, J.M., Alvarez, L.J., Candia, O.A. 1988. Cellular pH and Na^+–H^+ exchange activity in lens epithelium of Bufo marinus toad. *Am. J. Physiol.* **255:**C595–C602

Wolosin, J.M., Alvarez, L.J., Candia, O.A. 1990. HCO_3-transport in the toad lens epithelium is mediated by an electronegative Na^+-dependent symport. *Am. J. Physiol.* **258(27):**C855–C861